(This is a sample cover image for this issue. The actual cover is not yet available at this time.)

Journal of Theoretical Biology 303 (2012) 110–118

Contents lists available at SciVerse ScienceDirect

Journal of Theoretical Biology

journal homepage: www.elsevier.com/locate/yjtbi

Modeling fusion of cellular aggregates in biofabrication using phase field theories

Xiaofeng Yang [a], Vladimir Mironov [b,c], Qi Wang [a,d,*]

[a] Department of Mathematics and Nanocenter at USC, University of South Carolina, Columbia, SC 29208, USA
[b] Department of Material Science, Technical University of Vienna, Vienna, Austria
[c] Cuspis LLC, Charleston, SC, USA
[d] School of Mathematics, Nankai University, Tianjin 300071, PR China

ARTICLE INFO

Article history:
Received 22 September 2011
Received in revised form
21 February 2012
Accepted 1 March 2012
Available online 13 March 2012

Keywords:
Cellular aggregates
Tissue
Fusion
Phase field
Spectral methods

ABSTRACT

A mathematical model based on the phase field formulation is developed to study fusion of cellular aggregates/clusters. In a novel biofabrication process known as bioprinting (Mironov et al., 2009a), live multicellular aggregates/clusters are used to make tissue or organ constructs via the layer-by-layer deposition technique, in which the printed bio-constructs are embedded in hydrogels rich in maturogens and placed in bioreactors to undergo the fusion process of self-assembly, maturation, and differentiation to form the desired functional tissue or organ products. We formulate the mathematical model to study the morphological development of the printed bio-constructs during fusion by exploring the chemical–mechanical interaction among the cellular aggregates involved. Specifically, we treat the cellular aggregates and the surrounding hydrogels as two immiscible complex fluids in the time scale comparable to cellular aggregate fusion and then develop an effective mean-field potential that incorporates the long-range, attractive interaction between cells as well as the short-range, repulsive interaction due to immiscibility between the cell and the hydrogel. We then implement the model using a high order spectral method to simulate the making of a set of tissues/organs in simple yet fundamental geometries like a ring, a sheet of tissues, and a Y-shaped, bifurcating vascular junction by the layer-by-layer deposition of spheroidal cellular clusters in the bioprinting technology.

1. Introduction

Tissue fusion is an ubiquitous phenomenon during embryonic development and morphogenesis (Pérez-Pomares and Foty, 2006). The natural tissue fusion in vivo usually occurs in two steps. It starts from the initial tissue opposition and follows by sequential actual tissue fusion after establishing direct contacts between adjacent embryonic tissues. The impaired tissue fusion process during embryonic development can result in embryonic malformation and defects such as cleft palate. In the past, bioengineering processes have been devised to fabricate tissues under controlled conditions using tissue self-assembly, in which one seeds cells into biodegradable polymer scaffolds or gels, which are then cultured in bioreactors for several weeks and finally implanted into the recipient organism, where the maturation of the new organ takes place (Jakab et al., 2004; Marga et al., 2007).

In a novel biomimetic biofabrication process, called "bioprinting", multicellular tissue spheroids or aggregates are used as fundamental building blocks to construct the 3D tissue or organ (Griffith and Naughton, 2002; Jakab et al., 2004; Marga et al., 2007; Mironov et al., 2009a). The multicellular aggregates are first prepared in the form of tissue spheroids that consist of thousands of cells blended with bio-compatible hydrogels. They are then directly deposited by computer-aided design tools into desired 3D tissue or organ constructs via the layer-by-layer deposition technique. The printed bio-constructs immersed in a hydrogel are then placed in bio-incubator for maturation. During the incubating process, the cellular aggregates immersed in compatible hydrogel are expected to fuse into a 3D tissue or organ following the natural rule of histogenesis and organogenesis (Jakab et al., 2004; Neagu et al., 2005; Jakab et al., 2006, 2008). During this process, tissue self-assembly, fusion, differentiation and maturation take place. For instance, experimental evidence demonstrates that setting lumenized vascular tissue spheroids in a roll, as the result of tissue fusion, a lumenized vascular tube can be formed (Mironov et al., 2009a). Tissue fusion driven is a fundamental biophysical process in emerging organ bioprinting technology.

* Corresponding author. Tel.: +86 850 443 0294.
E-mail address: qwang@math.sc.edu (Q. Wang).

0022-5193/$ - see front matter © 2012 Elsevier Ltd. All rights reserved.
doi:10.1016/j.jtbi.2012.03.003

The bio-constructs ranging from the ones comprised tissue spheroids to functioning tissues or organs all exhibit fluid behavior during tissue fusion processes and are bona fide soft materials with various degrees of viscoelasticity. Numerical simulations of the morphogenesis phenomenon in bioprinting using the Monte Carlo method and experimental evidences (Jakab et al., 2004, 2006, 2008; Neagu et al., 2005, 2006; Marga et al., 2007) pointed out the strong influence of surface tension to the tissue spheroids fusion in the biofabrication process when the biomaterials (tissue spheroids and hydrogels) are regarded as viscous fluids. A separate study using experimental methods and numerical simulation with the cellular Potts model also explored the effect of surface tension and the hydrodynamics to the rounding of cell aggregate (Mombacha et al., 2005). The experimental evidence and the Monte Carlo simulation also demonstrate an interesting compaction phenomenon observed initially in the self-assembly of the bio-construct before it evolves into a smooth tissue or organ (Marga et al., 2007; Mironov et al., 2009b; Visconti et al., 2010; Ramirez and Angelini, 2010). This phenomenon resembles the long rang attractive interaction among small particles, but it occurs at a much large length and time scale. The molecular origin of the compaction can be the consequence of cell motility or chemically induced electrostatic interaction between cells mediated by the hydrogel. At large length and time scales, the phenomenon can be modeled using a coarse–grain model featuring the long range multicellular aggregate–aggregate interaction, which will be detailed in the next section.

It is known that cell aggregates exhibit fluid-like behavior during the tissue fusion process at large length and time scales (Marga et al., 2007). Both the multicellular cell aggregates in the form of tissue spheroids and the hydrogel in which the tissue spheroids are embedded are multiphase complex fluids in nature. Together, they form a coarse–grain binary complex fluid system, in which one fluid is the cellular aggregates and the other is the hydrogel. The dynamics of the binary fluid system can then be modeled in the coarse–grain length scale by models suitable for multiphase complex fluids. Given the large time scale in tissue fusion, elasticity of the tissue spheroids and the bio-constructs made up of the tissue spheroids can be effectively ignored unless an imposed external field is introduced. We therefore, model the bio-constructs at this time scale approximately as viscous fluids.

An excellent review for biofabrication methods, physical mechanisms and the discussion on the fluidity cellular aggregates is available in Marga et al. (2007). An elasto-visco-plastic continuum model is developed to investigate the cell aggregate deformation properties in tension (Preziosi et al., 2010), in which a trigger for yield stress is implemented. In large time scale, the model reduces to the viscous limit as well. The biophysical and biochemical mechanism of tissue fusion process is not fully understood. Modern mathematical modeling and computer simulation opens unique opportunities for explaining physical nature of tissue fusion process and predicting possible undesirable outcomes which is essential for designing optimal bioprinting protocol.

Modeling and simulating immiscible multiphase fluid flows have been challenging both mathematically and technically over the years. Various mathematical theories and computational technologies have been developed to tackle the problem. The front tracking method (Du et al., 2006), boundary integral method (Hou et al., 2001), level-set method (Sethian, 1999; Osher and Fedkiw, 2003), volume-of-fluid method (Hirt and Nichols, 1981), immersed-boundary method (Peskin, 1981; Leveque and Li, 1994), and phase field method (Anderson et al., 1998; Yue et al., 2004, 2005; Yang et al., 2006) have all been proposed, implemented and refined in a wide range of immiscible multiphase fluid flow applications, each of which has shown effectiveness in designated applications. Some of the methods are comparable in design concept while others can be combined to yield more effective computational technology (Kim et al., 2001). Among all methods listed above, the phase field method for multiphase fluid flows is perhaps the simplest to implement, given that the phase boundary is embedded in a level set of the phase variable governed by a dissipative evolutionary equation, and also the most physically relevant. Because of the ease of use, simplicity and relevance to material's physics, refined details in the formulation of the phase field equation can be carefully carved out and the free energy, especially, the interfacial free energy for the multiphase fluid can be devised properly to ensure accuracy in numerical computations and fidelity in physical modeling.

In an immiscible binary fluid, the phase field method employs a phase variable $0 \le \phi \le 1$ to track each phase in the binary fluid: $\phi = 1$ describes the phase of fluid I and $\phi = 0$ denotes the one occupied by fluid II while $0 < \phi < 1$ describes the interfacial region. The phase variable is also known as a labeling function for identification purposes. The time evolution of the phase variable ϕ is governed according to the Cahn and Hilliard (1958, 1959) equation:

$$\frac{d\phi}{dt} = \nabla \cdot (\lambda \nabla \mu), \tag{1.1}$$

where λ is proportional to the mobility and μ is the chemical potential of the multiphase fluid system, a functional of the phase variable ϕ, and $d\phi/dt$ is the material derivative. The phase variable ϕ can be identified with the volume fraction of fluid I; so, $1-\phi$ serves as the volume fraction of fluid II. In this formulation of the transport equation for ϕ, the flux of ϕ is assumed to be proportional to the force due to the prescribed chemical potential. However, a more physically appropriate assumption is to assume the excessive transporting velocity of ϕ, in addition to the bulk/average velocity, is proportional to the force due to the chemical potential, a consequence of the friction dynamics (Doi and Edwards, 1986; Bird et al., 1987). This leads to the singular or modified Cahn–Hilliard equation

$$\frac{d\phi}{dt} = \nabla \cdot (\lambda_s \phi \nabla \mu), \tag{1.2}$$

where λ_s is the mobility. If we assume mixing only takes place in the interfacial layer, it would be reasonable to assume $\lambda_s = \lambda_s^1(1-\phi)$, where λ_s^1 is a constant. Hence, the volume fraction will retain a constant within the bulk of each fluid. In the classical Cahn–Hilliard equation, λ is a constant; whereas it is a phase variable dependent function in the modified case. As $\lambda \to 0$, the transport equation for the phase variable reduces to a pure transport equation for the phase boundary which is commonly used in the level-set method (Sethian, 1999; Osher and Fedkiw, 2003).

The phase field model, also known as the diffuse interface method, benefits from the dissipation mechanism in the transport equation for ϕ. There exists an interfacial layer in which two fluids mix due to dissipation. It is expected to maintain a constant value for the phase variable ϕ outside the layer. For a slowly varying interface, namely, the interface with a small or intermediate curvature, phase field models yield acceptable interfaces with thickness controlled within a few grid points. When the curvature becomes large, resolving the interfacial layer accurately becomes a challenge. Nonetheless, the material system consisting of cellular aggregates and the host hydrogel matrix does not necessarily maintain a sharp interface at the coarse–grain level given the cell motility. Hence, the phase field method may serve as a good systematic way to model this biomaterial system.

To formulate the cellular spheroid fusion in a hydrogel matrix, we identify the cellular spheroid phase as fluid I and the ambient

fluid phase, the hydrogel, as fluid II in the framework of phase field theories. We account for three distinct interaction forces between these two "immiscible" fluids. Firstly, we introduce a short-range repulsive bulk potential to maintain the clear separation between the two distinctive fluid phases, a force to maintain immiscibility between the two fluids; secondly, we use a configurational entropic term in the interaction potential to describe the philic interaction between the cellular spheroids in close proximity and the resultant surface tension when coupled with the bulk potential; thirdly, we incorporate a *long-range* attractive interaction potential based on collective Lennard-Jones interaction among the cells physically. The third force is necessary to model the compaction process observed in the initial self-assembly process of cellular aggregates. This new force included in this phase field model can be viewed as a collective interaction between cells within a cellular aggregate and across cellular aggregates as the result of cell–cell attractive interaction among like cells mediated by the hydrogel. The genesis of the force is yet clear, but its existence is experimentally evident (Mironov et al., 2009a). Our phase field model is primarily developed based on these interaction forces and their coupling with the mass and momentum transport of the binary fluid system. Should additional forces between the adjacent cellular spheroids be identified experimentally at the cellular level, a potential yielding the mean force can be derived accordingly.

We organize the rest of the papers into three sections. In the second section, we derive the detailed phase field model and discuss its nondimensionalization. In the third section, we design an efficient high order numerical scheme to discretize the governing system of partial differential equations and discuss the numerical implementation that simulates the cellular cluster fusion process to form tissues and organs. Tissues in simple geometries like rings, sheets are simulated along with bio-fabrication of bifurcating Y-shaped vascular veins via layer-by-layer deposition in the fourth section.

2. Mathematical formulation of the phase field model

We treat the cellular cluster as a blob of complex fluids and its surrounding hydrogel matrix as a viscous fluid. The cellular cluster along with the surrounding fluid then forms a binary fluid mixture of two immiscible fluids (i.e., hydrogels will not turn into cellular spheroids and vice versa). The binary fluid system is assumed incompressible, which is a reasonable approximation. We use a phase variable ϕ to label each fluid phase in the system:

$$\phi = \begin{cases} 1 & \text{in cellular cluster,} \\ 0 & \text{in host hydrogel matrix.} \end{cases} \tag{2.1}$$

We denote the average velocity of the fluid mixture by $\mathbf{u}$. The transport equation for the mass and momentum of the mixture system is governed respectively by the momentum balance and the continuity equation

$$\begin{cases} \rho \dfrac{d\mathbf{u}}{dt} = \nabla \cdot (\phi\tau_1 + (1-\phi)\tau_2) - (\nabla p + \phi \nabla \mu), \\ \nabla \cdot \mathbf{u} = 0, \end{cases} \tag{2.2}$$

where $\rho = \phi\rho_1 + (1-\phi)\rho_2$ is the effective density for the binary fluid, ρ_1, τ_1 and ρ_2, τ_2 are the density and the extra stress tensor for the fluid consisting of cellular clusters and the host fluid matrix, respectively, μ is the extended chemical potential of the mixture system given below, and p is the hydrostatic pressure. The chemical potential of the material system is calculated from the system's free energy consisting of the extended "mixing free energy" (Doi, 1995; Flory, 1953) defined by

$$F_{mix}(\phi) = \frac{k_B T}{2} \int_\Omega (\gamma_1 |\nabla \phi|^2 + \gamma_2 F(\phi))\, dx, \tag{2.3}$$

where Ω is the domain that the mixture occupies, $F(\phi) = \phi^2(1-\phi)^2$ is the Ginzburg–Laudau double well potential, k_B is the Boltzmann constant, T is the temperature, γ_1 is a parameter measuring the strength of the conformation entropy and γ_2 is the strength of the bulk mixing free energy. This potential features a conformation entropic contribution which is universal among all molecules and a hydrophobic contribution due to the immiscibility between the hydrogel and the cells. On top of that, we introduce an additional interaction potential due to the long-range cellular interaction:

$$F_{cel}(\phi) = \int_\Omega \left(\frac{1}{2} \int_\Omega \chi(|x-y|)\phi(x,t)\phi(y,t)\, dy \right) dx. \tag{2.4}$$

We assume that the long-range cellular cluster interaction is due to the collective attractive interaction between the like cells parametrized by the Lennard-Jones potential $\chi(r)$ with

$$\chi(r) = V_{LJ}(r) = 4\epsilon \left(\left(\frac{\sigma}{r}\right)^{12} - \left(\frac{\sigma}{r}\right)^{6} \right), \tag{2.5}$$

where ϵ is a suitably chosen energy constant which is influenced by the cellular environment around the surface of the cellular cluster (i.e., it can be a feedback function should more detailed signaling molecular information becomes available when cellular clusters are placed in proximity), σ is the finite distance at which the inter-particle potential is zero and r is the distance between the interacting "particles" (cells) (Lennard-Jones, 1924). Like ϵ, σ is a parameter that depends on the detail of cellular interaction when used in this system. Thus, the total free energy of the system is then given by

$$F_{tot} = F_{mix} + F_{cel}. \tag{2.6}$$

The extended chemical potential for the material system is calculated by the variational derivative

$$\mu = \frac{\delta F_{tot}}{\delta \phi} = -\gamma_1 \nabla^2 \phi + \gamma_2 (1-\phi)\phi(1-2\phi) + \int_\Omega \chi(|x-y|)\phi(y,t)\, dy. \tag{2.7}$$

In practice, we use the truncated Lennard-Jones potential

$$\chi(r) = \begin{cases} V_{LJ}(r) - V_{LJ}(r_c), & r \le r_c, \\ 0, & r > r_c, \end{cases} \tag{2.8}$$

where $r_c \ge 2.5\sigma$. In the calculations we conducted in this paper, we used $r_c = 2.5\sigma$. We remark that the Lennard-Jones potential is attractive at the "long-range" and repulsive in the "short-range"; its use in this model is primarily for the "long-range" attractive effect. The short-range repulsive effect of the Lennard-Jones potential is easily offset by the conformational entropy which promotes a different kind of philic interaction at the short to mid-range interaction.

The phase variable ϕ or the volume fraction of the cellular component is transported via the Cahn–Hilliard equation

$$\frac{\partial \phi}{\partial t} + \nabla \cdot (\mathbf{u}\phi) = \nabla \cdot \lambda(\nabla \mu), \tag{2.9}$$

where λ is the mobility that is normally a function of the volume fraction ϕ. Often, it is replaced by a constant for simplicity. At the interface between the two fluid phases, from the Cahn–Hilliard equation, we identify the velocity of the cellular fluid as

$$\mathbf{u}_1 = \mathbf{u} - \frac{\lambda}{\phi} \nabla \mu \tag{2.10}$$

and that of the host fluid matrix as

$$\mathbf{u}_2 = \mathbf{u} + \frac{\lambda}{1-\phi}\nabla\mu. \tag{2.11}$$

These two velocities are identifiable only within the interfacial layer between distinctive phases or in their respective phase domain. Within each phase, we assume the complex fluid homogeneous.

The extra stress tensors are given according to the material's property of each fluid phase involved. Even though the multicellular cluster are non-Newtonian in nature, the rheological response in long time is approximately viscous or Newtonian. Considering the large time scale involved in the morphological development process, we assume both fluids viscous with distinct viscosities:

$$\tau_1 = 2\eta_1\mathbf{D}, \quad \tau_2 = 2\eta_2\mathbf{D}, \tag{2.12}$$

where η_1,η_2 are the viscosity for the cellular cluster fluid and the host fluid matrix, respectively, $\mathbf{D}$ is the rate of strain tensor for the mixture associated to the average velocity field $\mathbf{v}$ defined by

$$\mathbf{D} = \tfrac{1}{2}(\nabla\mathbf{u} + (\nabla\mathbf{u})^T).$$

We investigate the interfacial dynamics of the binary fluid associated with the cellular cluster fusion in a computational 2D domain $\Omega = [0,H]^2$ and 3D domain $\Omega = [0,H]^3$, respectively. At the boundary of the computational domain $\partial\Omega$, we impose no-flux boundary conditions for the phase variable of the cellular fluid, the Dirichlet boundary condition for the velocity:

$$\begin{cases} \nabla\phi\cdot\mathbf{n}|_{\partial\Omega} = 0, \\ (\mathbf{u}\phi - \lambda\nabla\mu)\cdot\mathbf{n}|_{\partial\Omega} = 0, \\ \mathbf{u}|_{\partial\Omega} = 0. \end{cases} \tag{2.13}$$

We use a characteristic time scale t_0 and a length scale h to nondimensionalize the variables

$$\tilde{t} = \frac{t}{t_0}, \quad \tilde{x} = \frac{x}{h}, \quad \tilde{\mathbf{u}} = \frac{\mathbf{u}t_0}{h}, \quad \tilde{p} = \frac{pt_0^2}{\rho_0 h^2}. \tag{2.14}$$

The length scale h is determined by the length scale of the bio-constructs that we simulate and the computational geometry that we choose while the time scale is done by either the growth time scale of the interface or the cellular cluster fusion time scale. The following dimensionless equations then arise:

$$\begin{aligned} &\Lambda = \frac{\lambda\rho_0}{t_0}, \quad \Lambda_s = \frac{\lambda_s\rho_0}{t_0}, \quad \Gamma_1 = \frac{\gamma_1 kTt_0^2}{\rho_0 h^4}, \\ &\Gamma_2 = \frac{\gamma_2 kTt_0^2}{\rho_0 h^2}, \quad Re_2 = \frac{\rho_0 h^2}{\eta_2 t_0}, \quad Re_1 = \frac{\rho_0 h^2}{\eta_1 t_0}, \\ &\tilde{\rho} = \phi\frac{\rho_1}{\rho_0} + (1-\phi)\frac{\rho_2}{\rho_0}, \quad \tilde{\epsilon} = \frac{\epsilon t_0^2}{\rho_0 h^2}, \quad \tilde{\sigma} = \frac{\sigma}{h}, \end{aligned} \tag{2.15}$$

where Re_1 and Re_2 are the Reynolds numbers for the cellular fluid and the ambient fluid, respectively, ρ_0 is an average (or a constant reference) density. For simplicity, we drop the $\tilde{}$ on the dimensionless variables and the parameters. The system of governing equations for the binary fluid in these dimensionless variables is given by

$$\rho\frac{d\mathbf{u}}{dt} = \nabla\cdot(\phi\tau_1 + (1-\phi)\tau_2) - (\nabla p + \phi\nabla\mu), \tag{2.16}$$

$$\nabla\cdot\mathbf{u} = 0, \tag{2.17}$$

$$\frac{\partial\phi}{\partial t} + \nabla\cdot(\phi\mathbf{u}) = \nabla\cdot(\Lambda\nabla\mu), \tag{2.18}$$

where

$$\tau_1 = \frac{2}{Re_1}\mathbf{D}, \quad \tau_2 = \frac{2}{Re_2}\mathbf{D}.$$

The dimensionless chemical potential is now given by

$$\mu = -\Gamma_1\nabla^2\phi + \Gamma_2\phi(1-\phi)(1-2\phi) + \int_\Omega \chi(|x-y|)\phi(y,t)\,dy. \tag{2.19}$$

3. Numerical methods

We apply the phase field model developed in the previous section to study fusion of the cellular clusters when they are embedded in a host hydrogel matrix, i.e., the time evolution of the overall exterior boundary of the cellular clusters arranged in a designer's pattern for tissue and organ generation. We first describe the numerical scheme to solve the Cahn–Hilliard equation without velocity (2.18), i.e. with a zero velocity field. This decoupled system is used to simulate the fusion of spheroids which are in contact initially. For this case, the bulk velocity remains near zero when fusion starts. Thus we only need to focus on the binary fluid evolution without significant fluid motion and employ the Cahn–Hilliard equation to investigate the interfacial dynamics from this moment on. Furthermore, we will discuss the numerical scheme to solve the coupled system of Cahn–Hilliard and Navier–Stokes equations (2.16)–(2.18) to investigate the hydrodynamic effect that drives cellular spheroid fusion when they are away from each other initially.

We denote $\Gamma = \Lambda\Gamma_1$ and $\eta = \sqrt{1/\Lambda\Gamma_2}$. The Cahn–Hilliard equation takes the following form:

$$\phi_t + \Gamma\Delta(\Delta\phi - (f'(\phi) + f_l)) = 0, \tag{3.1}$$

where

$$f'(\phi) = \frac{1}{\eta^2}(1-\phi)(1-2\phi)\phi, \quad f_l = \frac{1}{\Gamma_1}\int_\Omega \chi(|x-y|)\phi(y,t)\,dy.$$

We use the first-order backward Euler method to discretize the time derivative. The numerical scheme reads:

$$\frac{\phi^{n+1}-\phi^n}{\delta t} + \Gamma\Delta\Delta\phi^{n+1} - \frac{\Gamma S}{\eta^2}\Delta(\phi^{n+1}-\phi^n) = \Gamma\Delta(f'(\phi^n) + f_l(\phi^n)), \tag{3.2}$$

where the biLaplacian term is treated implicitly and all other nonlinear terms explicitly. An extra term associated with the artificial parameter S is introduced in order to balance the unstable constraint condition on the time step due to the explicit treatment of nonlinear terms (Shen and Yang, 2010). The spatial discretization of the semi-discrete equation is carried out using high order, spectral-Galerkin method with the Legendre–Gauss–Lobatoo points in one direction and Fourier method in the other two directions. Hence, in our implementations in 3D, the boundary condition in one direction is physical and the other two directions are periodic.

For the coupled system of Cahn–Hilliard equation and the Navier–Stokes equations (2.16)–(2.18), we use the first-order pressure-correction scheme developed in Chorin (1968, 1969), Temam (1969), and Guermond and Shen (2004). For simplicity, we assume the density of the cellular fluid and the hydrogel are the same and then set the "dimensionless density" $\rho = 1$ in our nondimensionalization. Assuming that $(\tilde{u}^n, u^n, p^n, \phi^n)$ is known, the numerical scheme consists of the following three steps:

1. *Update of the intermediate velocity field* $\tilde{u}^{n+1}$:

$$\begin{cases} \dfrac{\tilde{\mathbf{u}}^{n+1}-\mathbf{u}^n}{\delta t} - \left(\dfrac{1}{2Re_1} + \dfrac{1}{2Re_2}\right)\Delta(\tilde{\mathbf{u}}^{n+1}-\mathbf{u}^n) + \nabla p^n = N(\phi^n, \mathbf{u}^n), \\ \tilde{\mathbf{u}}^{n+1}|_{\partial\Omega} = 0, \end{cases} \tag{3.3}$$

where

$$(N(\phi,\mathbf{u}) = -\mathbf{u}\cdot\nabla\mathbf{u} - \frac{1}{\Lambda}\phi\nabla\mu + \left(\frac{\phi}{Re_1} + \frac{1-\phi}{Re_2} - \frac{1}{2Re_1} - \frac{1}{2Re_2}\right)\nabla^2\mathbf{u}$$

and

$$\mu = \frac{\Gamma}{\Lambda}\left[-\nabla^2\phi + \frac{1}{\eta^2}\phi(1-\phi)(1-2\phi) + \frac{1}{\Gamma_1}\int \chi(\mathbf{x}-\mathbf{y})\phi(\mathbf{y},t)\,d\mathbf{y}\right].$$

2. *Enforcing the divergence-free condition through projection to obtain velocity and pressure* (u^{n+1},p^{n+1}):

$$\begin{cases} \dfrac{\mathbf{u}^{n+1}-\tilde{\mathbf{u}}^{n+1}}{\delta t} + \nabla(p^{n+1}-p^n) = 0, \\ \dfrac{\partial(p^{n+1}-p^n)}{\partial n}\partial\Omega = 0. \end{cases} \tag{3.4}$$

3. *Update the phase variable* ϕ^{n+1}:

$$\begin{cases} \dfrac{\phi^{n+1}-\phi^n}{\delta t} + \tilde{\mathbf{u}}^{n+1}\cdot\nabla\phi^n + \Gamma\Lambda\Delta\phi^{n+1} \\ \quad -\dfrac{\Gamma S}{\eta^2}\Lambda(\phi^{n+1}-\phi^n) = \Gamma\Lambda(f'(\phi^n)+f_l(\phi^n)), \\ \dfrac{\partial\phi^{n+1}}{\partial n}\partial\Omega = 0, \quad \dfrac{\partial\Delta\phi^{n+1}}{\partial n}|_{\partial\Omega} = 0, \end{cases} \tag{3.5}$$

where $\mathbf{n}$ is the outward normal of the computational domain boundary. We implemented the coupled system in 2D and the decoupled system in full 3D. In the 2D numerical results presented below, we use 257 legend basis in one direction and 257 Fourier modes in the other direction. In the 3D simulations, we use 129 Fourier modes for the extra direction. The computational domain is scaled to $[-1,1]\times[-1,1]$ for the 2D case and $[-1,1]\times[-1,1]\times[-1,1]$ for the 3D case. For the 2D coupled model (2.16)–(2.18), we set the parameters in the momentum equations as $Re_1 = Re_2 = 10^{-10}$. In all simulations, we always fix $\Gamma = 10^{-4}$, $\eta = 0.01$, $\Gamma_1 = 10^7$, $\Gamma_2 = 10^{11}$, $S = 2$, $r_c = 0.5$, $\epsilon = 0.0005$, $\sigma = 0.2$. The numerical code converges spatially at the exponential order if the functions are smooth. Fig. 1 depicts a numerical convergence test that clearly demonstrates the first-order temporal convergence.

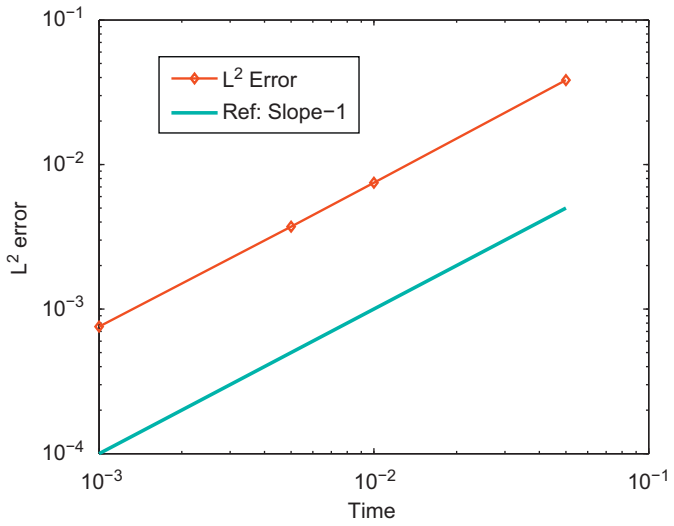

Fig. 1. Time convergence rate of the L^2 error of the phase field variable where the numerical solution uses 512^2 spatial grids and time step $\delta t = 0.0001$ as the exact solution.

4. Results and discussions

We next investigate cellular spheroid fusion with the numerical codes developed in the previous section. We first look into the compaction phenomenon in bioprinting of tissues using the 2D Cahn–Hilliard/Navier–Stokes solver. In the bioprinting process, when the cellular spheroids are deposited into a hydrogel to form a designed tissue construct, the cellular clusters undergo an initial compaction before fusing. During the compaction process, the center of mass of each cellular spheroid moves towards the geocenter of the bio-construct under a long-range attractive force. This motion occurs on a longer time scale than that of the fusion process. As an illustration, we simulate the evolution of a ring shaped bio-construct during the biofabrication process. Then, we simulate the fusion process for the cellular spheroids already in contact using the 3D Cahn–Hilliard solver for a set of bio-constructs in various geometries.

4.1. Initial attractive motion of cellular spheroids in tissue ring formation

The bio-construct made of the cellular spheroids with the spheroids initially positioned slightly apart undergoes a structural contraction globally. This is shown experimentally in Jakab et al. (2004) as the compaction phenomenon. We first examine this phenomenon using the 2D Navier–Stokes/Cahn–Hilliard solver. We investigate how the attractive motion of the cellular spheroids deposited in a ring pattern evolves in time. The layout of the ring construct consists of eight cellular spheroids positioned slightly apart. Fig. 2 depicts the configurational layout of the eight cellular spheroids at a series of snapshots of the simulation. At the initial stage of fusion, the center of mass of each spheroid moves towards the geocenter of the system under the long-range attractive interaction among the cells leading to an evolved ring pattern with the cellular spheroids in contact to each other. As soon as the spheroids get in contact with one another the philic interaction due to the conformational entropy takes over. A smooth tissue ring consisting of the cells forms under the dominating impact of the hydrodynamic surface tension. Given the fact that the volume of the cellular region is conserved in the model, the radius of the smoothed ring keeps shrinking. The radius reduction in time until the spheroids are in contact is recorded in Fig. 3, which agrees qualitatively with Mironov et al. (2009b). The continuing ring shrinking phenomenon during fusion after the cellular spheroids are in contact will be discussed in more details next.

This simulation demonstrates the effect of the long-range attractive interaction among the cells to the initial configurational evolution of the cellular spheroids within a designed bio-construct. For closely packed spheroids that are already in contact this effect is secondary. The primary force in that situation is the "philic" conformational entropic one closely related to the surface tension effect. Therefore, in the following simulation, we will instead focus on the interaction dominated by the surface tension effect in the spheroid fusion process upon contact in 3D. We also investigated the effect of the materials' properties to the compaction process. Evidently, the viscosity of the cellular aggregates and the hydrogel matrix can both retard the process. The motility constant Λ can also retard (at a smaller value) or accelerate (at a larger value) the process.

4.2. Morphological evolution of a ring construct made of cellular spheroids

Using the 3D Cahn–Hilliard solver, we investigate how a tissue ring can be fabricated by depositing a ring of cellular spheroids in

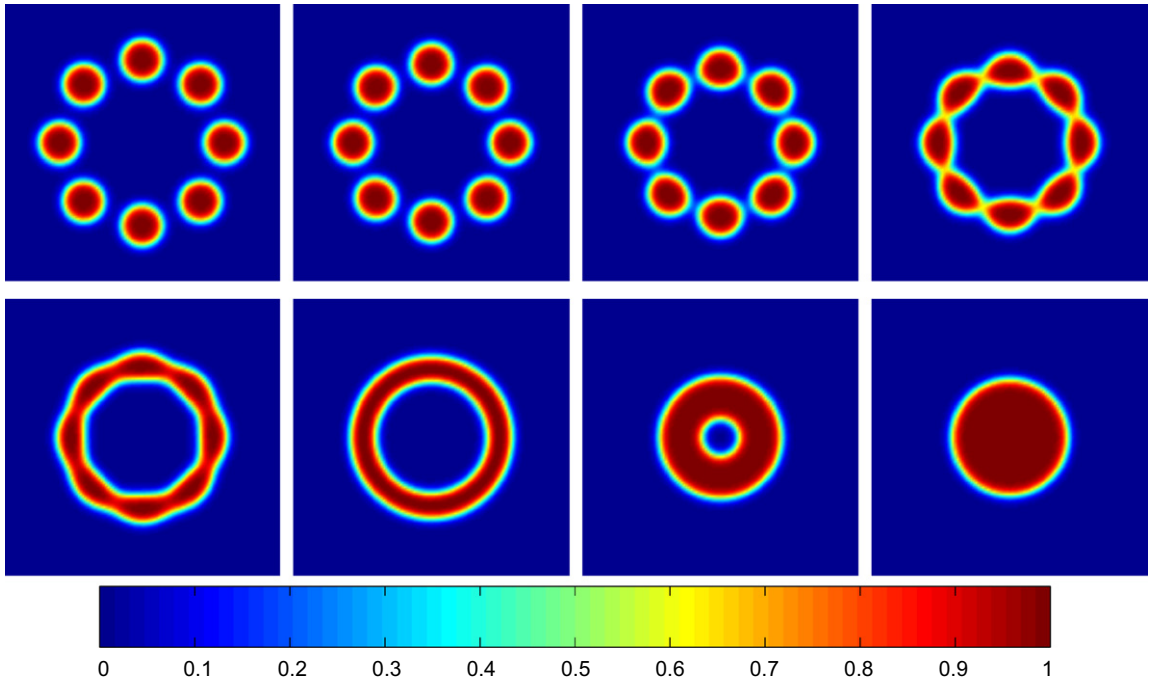

Fig. 2. Fusion of a ring construct from eight deposited spheroidal cellular clusters. Initially, the eight spheroids are placed equidistance to the geocenter and completely separated from each other. The long range like cell attractive force moves the center of mass of each spheroid towards the geocenter. Later, surface tension takes over to facilitate the fusion process. The snapshots are for $t=5$, 40, 55, 57, 58, 60, 80, 85.

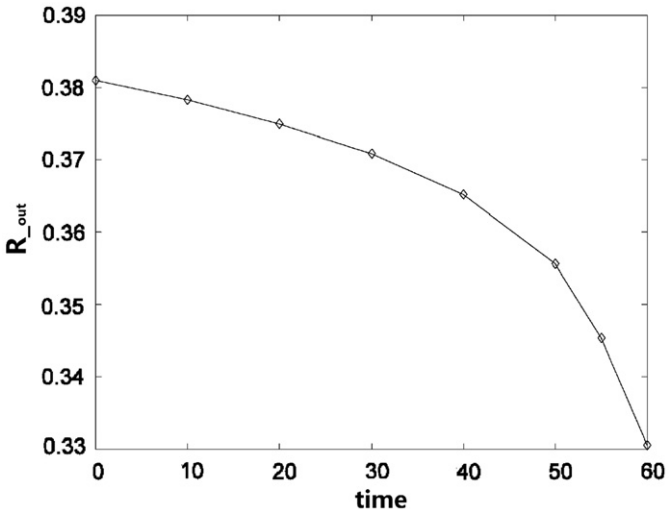

Fig. 3. The external radius of the ring construct as a function of time up to $t=60$. Compaction of the ring construct and later contraction of the smooth ring is evident.

contact in the bioprinting technology and then watch how this ring can eventually contract into a sphere over a long period of fusion process. The initial deposited cellular spheroids in a construct of the ring shape consists of eight spheroidal cell clusters. Due primarily to the philic effect, like cells tend to attract each other in long range (dissipation effect in coarse–grain) initially, the spheroids join into a corrugated ring; then, the surface tension takes over, the surface is gradually smoothed out. In the meantime the radius of the ring shrinks in order to maintain volume conservation. After sufficient long time, the ring collapses into a ball. Fig. 4 depicts five snapshots of the simulation at $t=0.1$, 2, 16, 30, 38, respectively. Compared with the fusion into a smooth ring construct, the evolution to contracting into a solid spherical ball takes much longer time as shown in Fig. 4.

4.3. Tissue sheet fabrication via single layer deposition of cellular spheroids

We then simulate the fabrication of a tissue sheet bio-construct via a single layer cellular spheroids deposition. We lay nine cellular spheroids initially on a flat surface in a square pattern. The bio-construct gradually joins into a networked construct with four visible holes. The entire sheet keeps contracting to close the holes and eventually leads to a solid sheet. The time scale for sealing the holes is longer than the time taken fusing the spheroids in contact to a smooth networked construct. The dissipation of the cellular material and the surface tension are the dominating mechanisms driving the fusion process. Fig. 5 depicts the simulation all the way to the moment a smooth, solid sheet is formed. The packing of the initial spheroids is not optimal though. If we pack the spheroids tightly, the fusion time can be reduced by 50% or more as will be shown in the next example. So optimal package can have a direct impact to the spheroid fusion process.

4.4. Lumenized tube generated via layer-by-layer deposition of cellular spheroids

To simulate the layer-by-layer deposition to fabricate the vascular vein or lumenized tube, we stack rings of spheroids one on top of the other up to three layers in our next simulation. The initially rugged tube construct evolves into a smooth tube with the walls thickened over time, which qualitatively captures the morphological evolution of the fusion process observed in experiments for tube formation (Fig. 6).

The positioning or packing of the spheroids relative to each other seems not to make a difference qualitatively. Quantitatively, however, a bio-construct with an initially more tightly packed spheroids can accelerate the fusion/maturation process significantly. Fig. 7 depicts fusion of a tightly packed spheroid tube construct, in which the tube fuses into a hole-less tube in much shorter time than the loosely packed tube construct depicted in Fig. 6.

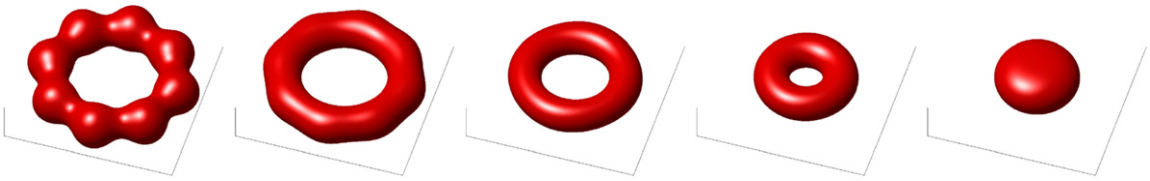

Fig. 4. Fusion of a ring construct from eight deposited spheroidal cellular clusters. Surface tension plays a major role in the fusion process. The snapshots are taken at $t=0.1$, 2, 16, 30, 38.

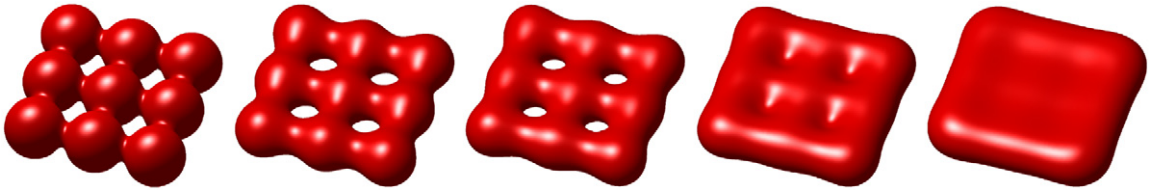

Fig. 5. A tissue sheet is simulated via fusion of a single layer deposited cellular spheroids. The snapshots are taken at $t=0$, 0.5, 1, 2, 3.

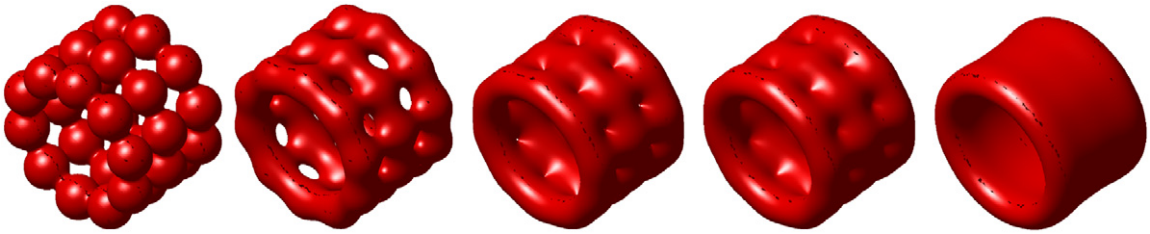

Fig. 6. Tube-formation in layer-by-layer deposition of cellular spheroids. Snapshots are taken at $t=0$, 0.1, 0.24, 0.25, 0.5. It is completely fused into a smooth tube at $t=0.25$.

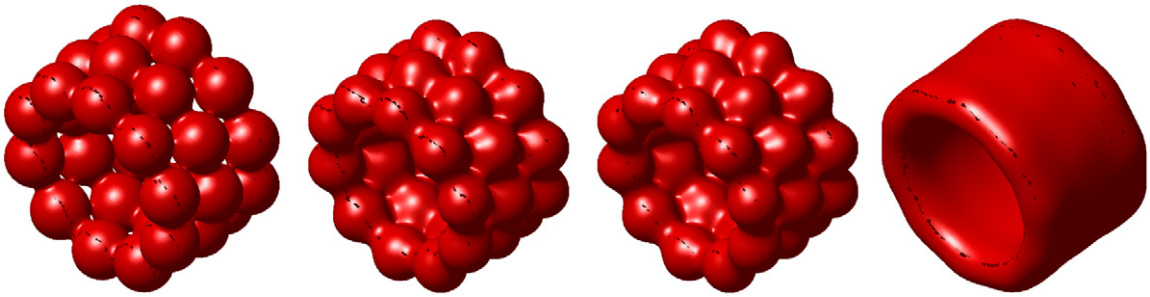

Fig. 7. Tube-formation in layer-by-layer deposition of cellular spheroids with nearly optimal packing. Snapshots are taken at $t=0$, 0.008, 0.009, 0.2. It is completely fused into a smooth tube at $t=0.009$. With an optimal packing, fusion can take place much quickly.

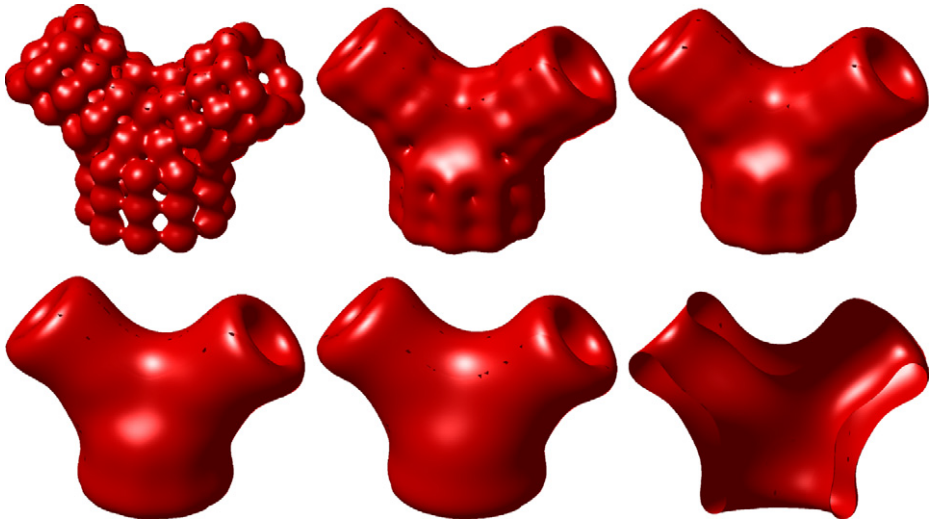

Fig. 8. Branching vascular vein simulated using the phase field model. Good branching vascular construct made of layer-by-layer deposition and strategic remedy for packing near the bifurcating point is achieved for a given initial profile. Snapshots are taken at $t=0$, 0.2, 0.3, 0.5, 0.8.

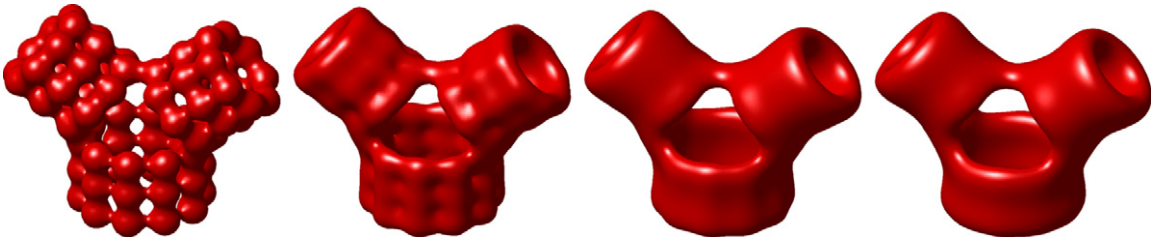

Fig. 9. Perforated tube made via layer-by-layer deposition of cellular spheroids with a bad packing strategy. A defective branching vascular construct forms, in which holes are present near the branching point. Snapshots are taken at $t=0$, 0.2, 0.4, 0.6.

4.5. Bifurcating vascular junction fabrication via layer-by-layer deposition of cellular spheroids

We extend the layer-by-layer deposition strategy to fabricating a bifurcating lumenized tube. If the initial deposition of the construct is done without defect, i.e., too large a hole in a later stage of fusion, both Y-shaped and T-shaped joints can be formed within the same period of time like a single lumenized tube. Fig. 8 depicts a Y-shaped bifurcating tube fabricated via fusion of packed cellular spheroids. If the initial deposition were not done properly, a defective bifurcating tube may also form as shown in Fig. 9, where permanent holes remain. Therefore, the initial deposition of the cellular spheroids are instrumental to ensure the quality of the final product. This numerical tool can then be used to study the correlation between the initial configuration of the spheroid arrangement and the possible final product defect due to the unexpected holes on the wall. Ultimately, it can be embedded in a computer-aided design software for the bioprinting fabrication.

5. Conclusion

We have developed a phase field model for studying fusion of cellular aggregates by treating the cellular aggregate and the host hydrogel matrix as two immiscible fluids. The model incorporates the long-range attractive interaction between adjacent cellular aggregates, philic (attractive) interaction in close contact and the repulsive interaction due to immiscibility of distinctive materials at the material's interface. An efficient, high order spectral method is employed to discretize the governing partial differential equation in the model. A numerical solver is developed by implementing the spectral method in 2D. A 3D numerical solver is developed based on the Cahn–Hilliard equation only to be applied to investigate the fusion process in which the cellular spheroids are placed in contact. Both solvers are then applied to simulate biofabrication of various specific geometric shaped tissues and organs via layer-by-layer deposition of spheroidal cellular clusters. The hydrodynamic effect involving momentum transport is shown to be important in the initial compaction process; it is later dominated by the philic interaction among the cells once the cellular clusters are in contact with each other. The time scale for fusion of the cellular clusters depends on the initial packing of the cellular spheroids. Tight packing will certainly result in shorter fusion time. The bifurcating bio-constructs also depend on the packing at the bifurcating point. A computer-aided design tool is therefore necessary to virtually simulate the entire biofabrication and provides guidance to the bioprinting process in precision.

Acknowledgments

Qi Wang's research is partly supported by National Science Foundation Grants CMMI-0819051 and DMS-0908330. Xiaofeng Yang's research is supported in part by the Army Research Office (ARO) W911NF-09-1-0389. Both are also partially supported by the SC EPSCOR GEAR program. The authors thank Drs. C. Drake, R.R. Markwald and X. Wen for their sharing of the experimental findings, vision, encouragement and guidance for this project.

References

Anderson, D.M., McFadden, G.B., Wheeler, A.A., 1998. Diffuse-interface methods in fluid mechanics. Annu. Rev. Fluid Mech. 30, 139–165.
Bird, R.B., Armstrong, R.C., Hassager, O., 1987. Dynamics of Polymeric Liquids, vols. 1 & 2. John Wiley and Sons, New York.
Cahn, J.W., Hilliard, J.E., 1958. Free energy of a nonuniform system. I: interfacial free energy. J. Chem. Phys. 28, 258–267.
Cahn, J.W., Hilliard, J.E., 1959. J. Chem. Phys. 31, 688–699.
Chorin, A.J., 1968. Numerical solution of the Navier–Stokes equations. Math. Comput. 22, 745–762.
Chorin, A.J., 1969. On the convergence of discrete approximations to the Navier–Stokes equations. Math. Comput. 23, 341–353.
Doi, M., 1995. Introduction to Polymer Physics. Oxford Science Publications, Oxford.
Doi, M., Edwards, S.F., 1986. The Theory of Polymer Dynamics. Oxford Science Publications, Oxford.
Du, J., Fix, B., Glimm, J., Jia, X., Li, X., Li, Y., Wu, L., 2006. A simple package for front tracking. J. Comput. Phys. 213 (2), 613–628.
Flory, P.J., 1953. Principles of Polymer Chemistry. Cornell University Press, Ithaca, NY.
Griffith, L.G., Naughton, G., 2002. Tissue engineering current challenges and expanding opportunities. Science 295, 1009–1014.
Guermond, J.L., Shen, J., 2004. On the error estimates of rotational pressure-correction projection methods. Math. Comput. 73, 1719–1737.
Hirt, C.R., Nichols, B.D., 1981. Volume of fluid (VOF) method for the dynamics of free boundaries. J. Comput. Phys. 39, 201–225.
Hou, T.Y., Lowengrub, J.S., Shelley, M.J., 2001. Boundary integral methods for multicomponent fluids and multiphase materials. J. Comput. Phys. 169 (2), 302–362.
Jakab, K., Neagu, A., Mironov, V., Markwald, R.P., Forgacs, G., 2004. Engineering biological structures of prescribed shape using selfassembling multicellular systems. Proc. Natl. Acad. Sci. USA 101, 2864–2869.
Jakab, K., Damon, B., Neagu, A., Kachurin, A., Forgacs, G., 2006. Three-dimensional tissue constructs built by bioprinting. Biorheology 43, 509–513.
Jakab, K., Norotte, C., Damon, B., Marga, F., Neagu, A., Besch-Williford, C.L., Kachurin, A., Church, K.H., Park, H., Mironov, V., Markwald, R., Vunjak-Novakovic, G., Forgacs, G., 2008. Tissue engineering by self-assembly of cells printed into topologically defined structures. Tissue Eng.: Part A 14 (3), 413–421.
Kim, J., Kim, D., Choi, H., 2001. An immersed-boundary finite-volume method for simulations of flow in complex geometries. J. Comput. Phys. 171, 132–150.
Lennard-Jones, J.E., 1924. On the determination of molecular fields. Proc. R. Soc. London A 106 (738), 463–477.
Leveque, R.J., Li, Z., 1994. The immersed interface method for elliptic equations with discontinuous coefficients and singular sources. SIAM J. Numer. Anal. 31, 1019–1044.
Marga, F., Neagu, A., Kosztin, I., Forgacs, G., 2007. Developmental biology and tissue engineering. Birth Defects Res. (Part C) 81, 320–328.
Mironov, V., Visconti, R.P., Kasyanov, V., Forgacs, G., Drake, C.J., Markwald, R.R., 2009a. Organ printing: tissue spheroids as building blocks. Biomaterials 30, 2164–2174.
Mironov, V., Zhang, J., Gentile, C., Brakkea, K., Trusk, T., Jakabb, K., Forgacsb, G., Kasyanov, V., Visconti, R.P., Markwald, R.R., 2009b. Designer blueprint for vascular trees: morphology evolution of vascular tissue constructs. Virtual Phys. Prototyping 4 (2), 64–74.
Mombacha, J.C.M., Robertb, D., Granerc, F., Gilletd, G., Thomase, G.L., Idiarte, M., Rieu, J.-P., 2005. Rounding of aggregates of biological cells: experiments and simulations. Physica A 352, 525–534.
Neagu, A., Jakab, K., Jamison, R., Forgacs, G., 2005. Role of physical mechanisms in biological self-organization. Phys. Rev. Lett. 95, 178104.
Neagu, A., Kosztin, I., Jakab, K., Barz, B., Neagu, M., Jamison, R., Forgacs, G., 2006. Computational modeling of tissue self-assembly. Mod. Phys. Lett. B 20 (20), 1217–1231.

Osher, S.J., Fedkiw, R.P., 2003. Level Set Methods and Dynamic Implicit Surfaces. Springer-Verlag.

Pérez-Pomares, J.M., Foty, R.A., 2006. Tissue fusion and cell sorting in embryonic development and disease: biomedical implications. Bioessays 28 (8), 809–821.

Peskin, C.S., 1981. The fluid dynamics of heart valves: experimental, theoretical and computational methods. Annu. Rev. Fluid Mech. 14, 235–259.

Preziosi, L., Ambrosi, D., Verdier, C., 2010. An elasto-visco-plastic model of cell aggregates. J. Theor. Biol. 262, 35–47.

Ramirez, C.H., Angelini, J.O., 2010. Morphogenesis in silico applied in bioprinting. In: Proceedings of the 6th Congress of Latin American Artificial Organs and Biomaterials. Gramado, Rio Grande do Sul, Brazil, August, pp. 1–12.

Sethian, J.A., 1999. Level Set Methods and Fast Marching Methods: Evolving Interfaces in Computational Geometry, Fluid Mechanics, Computer Vision, and Materials Science. Cambridge University Press.

Shen, J., Yang, X., 2010. Numerical approximations of Allen–Cahn and Cahn–Hilliard equations. Disc. Conti. Dyn. Sys. A. 28, 1669–1691.

Temam, R., 1969. Sur l'approximation de la solution des Sequations de Navier–Stokes par la methode des pas fractionnaires II. Arch. Ration. Mech. Anal. 33, 377–385.

Visconti, R.P., Kasyanov, V., Gentile, C., Zhang, J., Markwald, R.R., Mironov, V., 2010. Towards organ printing: engineering an intra-organ branched vascular tree. Expert Opinion Biol. Ther. 10 (3), 409–420.

Yang, X., Feng, J.J., Liu, C., Shen, J., 2006. Numerical simulations of jet pinching-off and drop formation using an energetic variational phase-field method. J. Comput. Phys. 218, 417–428.

Yue, P., Feng, J.J., Liu, C., Shen, J., 2004. A diffuse-interface method for simulating two-phase flows of complex fluids. J. Fluid Mech. 515, 293–317.

Yue, P., Feng, J.J., Liu, C., Shen, J., 2005. Viscoelastic effects on drop deformation in steady shear. J. Fluid Mech. 540, 427–437.